9. V. Varadarajan, K. Kim, and T. P. Bernat, *J. Vac. Sci. Technol. A* **5**, 2750 (1987).

10. L. S. Mok and K. Kim, *J. Fluid Mech.* **176**, 521 (1987).

11. K. Kim, L. Mok, M. J. Erlenborn, and T. P. Bernat, *J. Vac. Sci. Technol. A* **3**, 1196 (1985).

12. K. Kim, B. J. Smoot, R. L. Woerner, and C. D. Hendricks, *Appl. Phys. Lett.* **34**, 282 (1979).

13. S. Denus, W. Muniak, and E. Woryna, *Laser and Particle Beams* **7**, 15 (1989).

14. C. K. Immesoete, L. Forsley, S. Scarantino, and H. Kim, *J. Vac. Sci. Technol.* (to be published).

15. B. A. Brinker, J. M. Cavese, J. R. Miller, S. G. Noyes, S. Sheble, and L. T. Whitaker, *J. Vac. Sci. Technol. A* **1**, 941 (1983).

16. H. Kong, M. D. Wittman, and H. Kim (to be published); see following article [LLE Review **40**, 212 (1989)].

17. P. C. Souers, *Hydrogen Properties for Fusion Energy*, (University of California Press, Berkeley, 1986).

18. G. E. Childs and D. E. Diller, *Adv. Cryo. Eng.* **15**, 65 (1969).

2.C A New Shearing Interferometer for Real-Time Characterization of Cryogenic Laser-Fusion Targets

As discussed in the preceding article, direct-drive inertial confinement fusion targets require a cryogenically cooled spherical shell in which the DT fuel is condensed in a uniform layer on the inner wall. Optical interferometry is the predominant technique used to characterize the thickness and uniformity of the cryogenic fuel layer. In addition to inherent optical limitations such as spherical and chromatic aberration, many of the interferometers used in the past are vibration sensitive or do not possess the adjustment versatility necessary to effectively characterize cryogenic inertial fusion targets. This article describes a new and unique shearing interferometer developed at LLE and implemented on the OMEGA target chamber for real-time characterization of cryogenic inertial fusion targets along two orthogonal views.

The shearing cube interferometer[1] supplied to LLE with the cryogenic target system (developed and built by KMS Fusion) has several limitations. This system uses OMEGA focusing lenses to illuminate and image the fusion target and therefore requires retractable

mirrors to be inserted into the OMEGA beamline during target characterization. Although the interferometer was designed to take advantage of the light-collecting capability of the f/3 OMEGA focusing lenses, the fact that these mirrors must be retracted at least 10 s before the laser shot results in loss of information regarding the state of the target just prior to irradiation. Also, this interferometer analyzes the target only along a single view, which is insufficient to determine the uniformity of the fuel layer in three dimensions. Therefore, it was necessary to develop a dedicated interferometric system that could characterize the state of the target along two orthogonal directions up until a few milliseconds prior to the laser shot.

Several requirements must be met before a type of interferometry can be useful for cryogenic liquid-DT fusion experiments. The portion of the reference wave front used to produce the interferogram must be selectable, and conversion of the background from a constant phase to a high-spatial-frequency fringe pattern must be rapid and reliable. The ability to change between these two states rapidly is essential because a constant phase background is convenient for visual inspection of the overall uniformity and concentricity of the cryogenic DT layer; whereas a high-spatial-frequency fringe pattern is more useful for determining the thickness and local uniformity of the fuel layer.[2] In addition to these properties, the interferogram produced must have high-contrast fringes and the interferometer must be compact enough to be accommodated by the limited space available to a diagnostic on the OMEGA target chamber.

Many types of interferometers have been applied to and developed for investigating the thickness and uniformity of a cryogenic liquid-DT fuel layer condensed on the interior of a laser-fusion target. These interferometers may be classified into two main categories: (1) two-beam interferometry, including ordinary Mach-Zehnder interferometry[3,4] and holographic interferometry,[5–7] and (2) single-beam interferometry, such as rotational-shearing interferometry,[8] lateral-shearing interferometry[9] and wedge interferometry.[10] Two-beam interferometry is difficult to implement on the large scale required by fusion experiments because of its sensitivity to relative vibrations between the two beams. In addition to its extreme sensitivity to vibration, holographic interferometry has the disadvantage of not being a true real-time technique and registration of the hologram and the object under investigation must be precise and reproducible. Both lateral- and rotational-shearing interferometry are limited in that only a relatively small region of the reference wave front can be selected for interference, and their images contain distortion and spherical aberration due to the thick optical plates that must be inserted into the beam path, such as Dove-prisms or shearing cubes. Also, it is difficult to change the interferogram from a constant-phase background to one with high-spatial-frequency interference fringes. Finally, a wedge interferometer is limited by a nonselectable reference wave front and a background-fringe spatial frequency that is fixed by the wedge angle.

Upon realizing the limitations of existing interferometric methods with regard to our application, we sought to develop an alternative

interferometer. One desirable aspect of a shearing interferometer is that both the object and reference wave fronts traverse nearly the same optical path, making it virtually insensitive to vibration and air turbulence. A major asset of a Mach-Zehnder interferometer is that the reference wave fronts are truly plane parallel and their direction of propagation can be widely adjusted in angle with respect to that of the object wave fronts. By combining the desirable features of these two interferometers and eliminating their drawbacks, we have developed a new, compact, single-beam interferometric system that is less sensitive to environmental vibration than a two-beam system; has the ability to select a reference wave front and to change the background fringe frequency from zero to a high value; and has no distortion, chromatic, or spherical aberration. Also, it produces a high-contrast interferogram even with comparatively low target illumination—an important aspect in reducing the heat load on the cryogenic DT fuel.

The entire optical system consists of three subassemblies: (1) an input system to expand and collimate the laser light, (2) an optical-relay system to image the target remotely, and (3) the interferometer itself. A schematic of this system is shown in Fig. 40.24(a). The output beam from an Ar^+ laser (514 nm) is coupled to a single-mode optical fiber that acts as a spatial filter and allows the light to be easily transported to the wall of the OMEGA target chamber. The output end of the fiber is mounted on a multi-axis positioner such that it can be

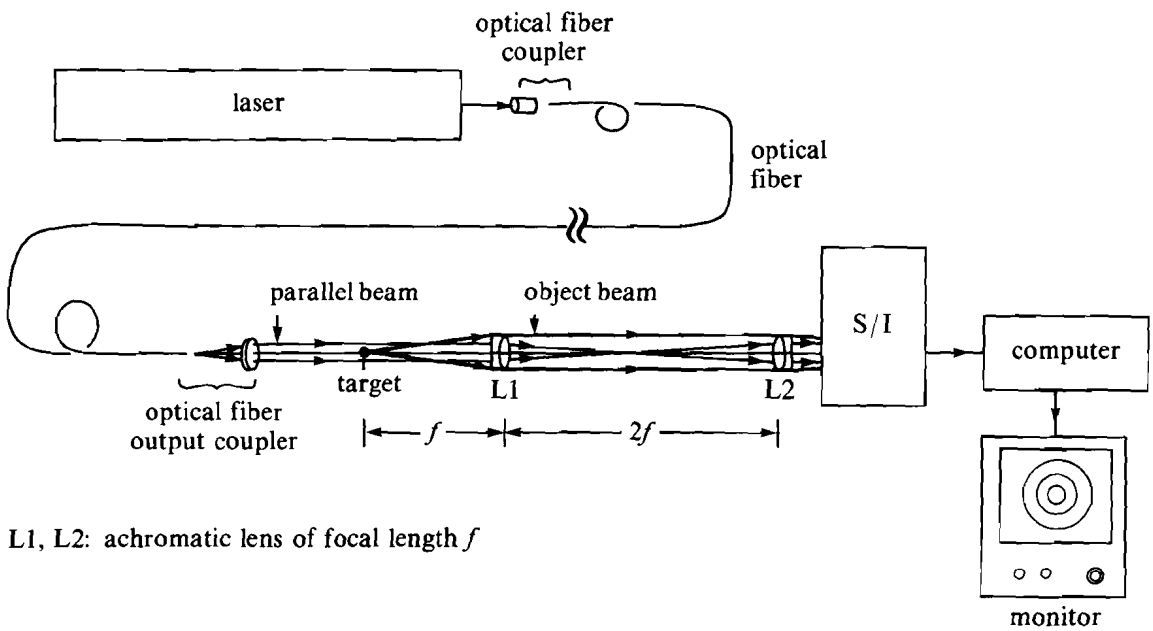

L1, L2: achromatic lens of focal length f

T908

Fig. 40.24(a)
Schematic diagram of the new shearing-interferometer optical system.

positioned with respect to a collimating lens for precise centering, pointing, and collimation of the filtered and expanded laser beam. The input assembly fits compactly onto a vacuum flange used to cover a 4-in. port on the OMEGA target chamber, and the lens itself serves as the vacuum window.

An optical-relay system is used to form an image of the target with a unity magnification. The resultant image is then magnified with a microscope objective lens (20×) onto a high-resolution CCD camera consisting of a 512 × 512 pixel array. The f/5.6 achromatic positive lenses used in the optical-relay system produce a theoretical resolution limit of 3.3 μm. Due to the finite pixel size, the camera approaches the resolution limit of the optical system when the field of view of the magnified image is about 1500 μm. The target image is focused by adjusting the position of the microscope objective lens, and the magnification of the image is controlled by the spacing between the microscope objective lens and the CCD array.

The output assembly, which houses the optical-relay system and supports the interferometer, was also designed around the space requirements of an OMEGA 4-in. port and the solid-angle constraints associated with it. It consists of a vacuum flange with provisions for rigidly mounting the interferometer base plate and a cylindrical tube that extends into the vacuum chamber. The axis of this tube defines the optical axis of the relay system and points directly at the target position at the center of the tank. The lenses are fixed at the desired spacing within the tube using machined shoulders and threaded retaining rings; and the lens farthest from the target also serves as the vacuum window. This feature eliminates the spherical aberration associated with converging or diverging wave fronts passing through a conventional parallel-plate vacuum window.

As shown in Fig. 40.24(b), the interferometer is placed between the optical-relay system and the microscope objective lens. At this position, the portion of the wave front that did not interact with the target is again collimated and the wave front that contains the phase information due to its passage through the target is converging to a focus in front of the microscope objective. The passage of light through the interferometer is as follows: The light emerging from the optical-relay system is split 50/50 in amplitude. The reflected beam from the beam-splitter surface that is reflected again by mirror *M*1 and the transmitted beam through the beam splitter that is reflected by mirror *M*2 are designated by *wf*-1 and *wf*-2 respectively. Each of these two wave fronts is composed of a plane-parallel wave front and the phase information of the target. *Wf*-1 undergoes only first-surface reflections as it passes through the interferometer, so that it is aberration-free upon interacting with its optical components. *Wf*-2 is transmitted twice through the beam splitter so that its image wave front is distorted; however, its plane-parallel component is aberration-free because the plane wave fronts are not distorted by the parallel plate.

The tilt and phase control of the interferometer is done by adjusting *M*2 only; therefore, one can obtain or select the desired interferogram

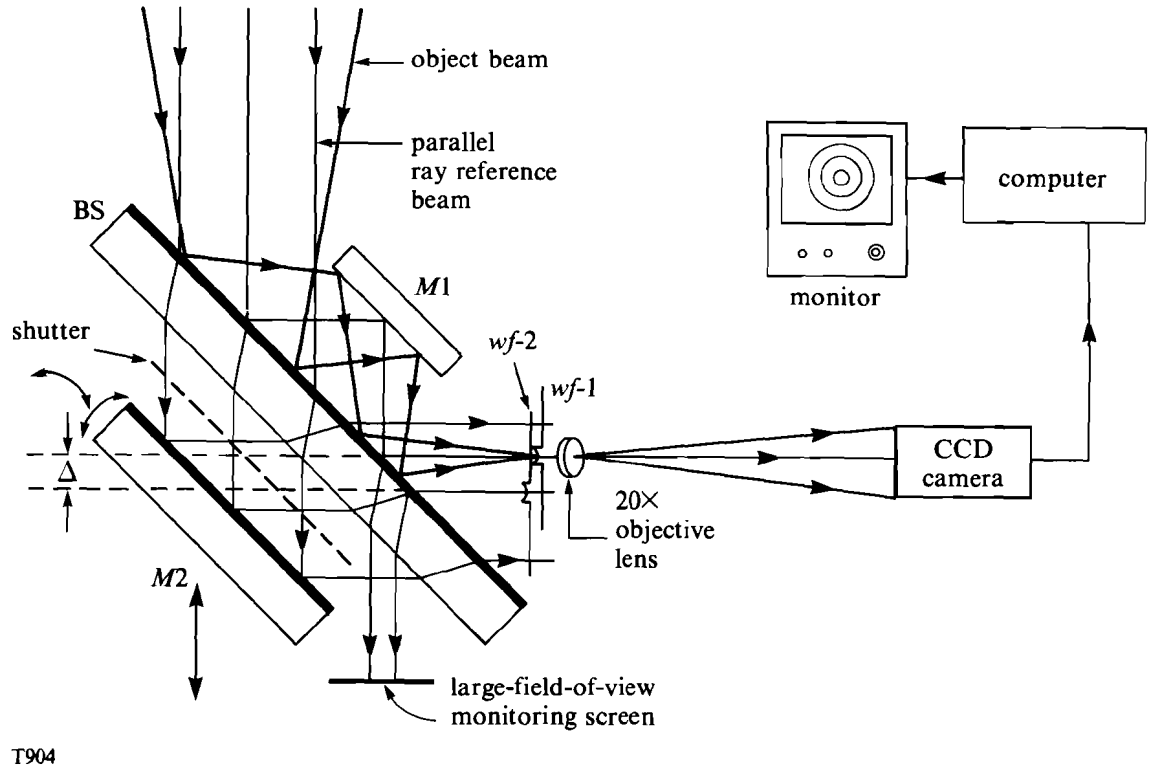

Fig. 40.24(b)
Detailed schematic diagram of the shearing interferometer showing the passage of the object and reference wave fronts through it.

without further alignment of the optical system by repositioning or refocusing the image. This mirror can be rotated about two orthogonal axes that allow the tilt fringes to be oriented along any direction and adjusted continuously in spatial frequency from 0-2000 lines/mm, and also allows one to obtain a very accurate constant background-phase interferogram with a tilt angle $\theta_t < 25$ μrad ($\lambda/40$). This highly accurate alignment is accomplished by using the large-field-of-view interferogram produced by reflection at the beam-splitter surface where *wf*-1 and *wf*-2 recombine as shown in Fig. 40.24(b). Phase control is accomplished by translating *M*2 with respect to the beam-splitter surface; and the minimum phase control is $<\lambda/20$ using a differential micrometer. This phase control allows the precise positioning of the tilt fringes or selection of the background phase when tilt is absent from the interferogram. Selection of the reference wave front is also one dimensionally possible by translating *M*2 by an amount Δ as shown in Fig. 40.24(b) ($0 \leq |\Delta| < 20$ mm). The fact that this is a single-beam interferometer and one that possesses the ability to select a portion of the reference beam that passes near the target to form the interferogram greatly reduces the effects of vibration, air turbulence, and imperfections in the optics that would normally tend to degrade the image.

Figure 40.25(a) shows *wf*-1 and *wf*-2 interfering with each other at the focal point of the optical-relay system. While *wf*-1 is aberration-free, *wf*-2 contains a distorted image but possesses an otherwise aberration-free plane-parallel wave front. Interference fringes appear where the optical path differs by integral multiples of the wavelength used (λ_o) as shown in Fig. 40.25(a). Figures 40.25(b) and 40.25(c) are interferograms obtained when the tilt angle (θ_t) is zero and nonzero respectively. The bull's-eye pattern [Fig. 40.25(b)] is useful for visual inspection of the target uniformity and concentricity, whereas the high-spatial-frequency background pattern [Fig. 40.25(c)] is more suited for detailed two-dimensional calculations of the target's fuel-layer thickness. If a shutter is placed between the beam splitter and mirror *M2*, thus blocking the reference beam, the object beam alone can be imaged, as shown in Fig. 40.25(d). This shadowgram is mainly used for sharply focusing the image onto the CCD detector and positioning it in the field of view, but it can also be used for roughly determining the uniformity and concentricity of the fuel layer. To convert from one type of image to another takes only a few seconds. All of the images have clear outer boundaries, which indicates that they are aberration-free. Each image has a dark band in its outer region that is due to the vignetting effect of the limited aperture size of the f/5.6 optical-relay system.

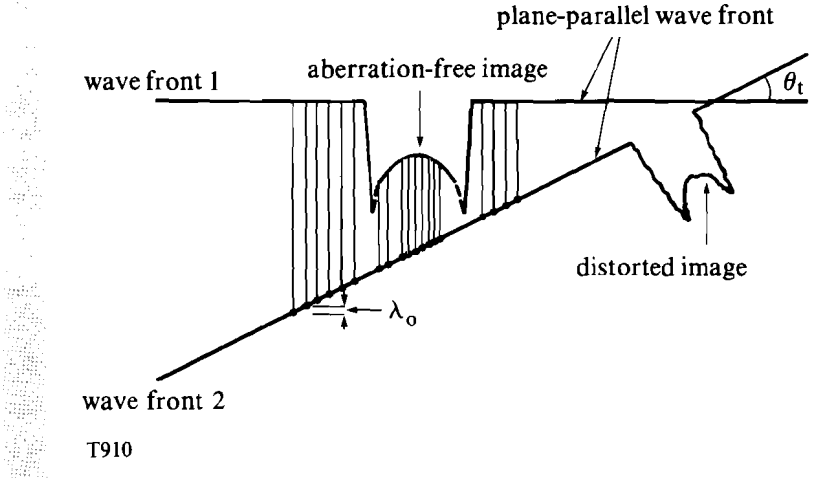

Fig. 40.25(a)
Interference of the object and reference wave fronts at the focal point of the optical-relay system. The parallel lines indicate where the fringes would appear.

In conclusion, we have developed a shearing interferometer that produces an aberration-free interferogram. The interferometer is achromatic, which is essential for obtaining interferograms of several different wavelengths to determine the DT-layer thickness and fractional condensation of the fuel. Two shearing interferometers have been implemented on the target chamber of the OMEGA laser system

to provide orthogonal views of the cryogenic target during experiments. Both of the interferometers can be focused remotely and have remotely controlled shadowgram shutters. The tilt and phase adjustment of one of the interferometers can also be remotely controlled.

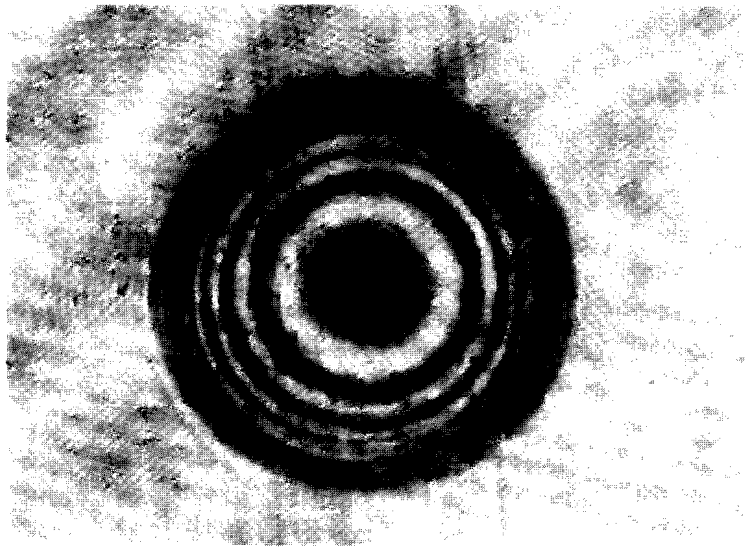

T911

Fig. 40.25(b)
Interferogram of a cryogenic liquid-layer inertial-fusion target using a constant background phase ("bull's-eye" pattern). The glass microballoon has an outer diameter of 262 μm and a wall thickness of 3.8 μm. It contains an equimolar ratio of deuterium and tritium and was filled to a room-temperature pressure of 100 atm.

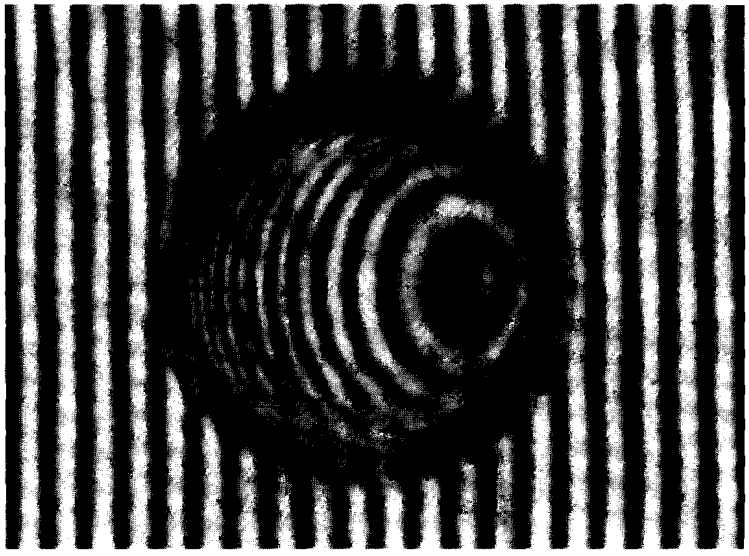

T912

Fig. 40.25(c)
Interferogram of the same target with a high-spatial-frequency background-fringe pattern.

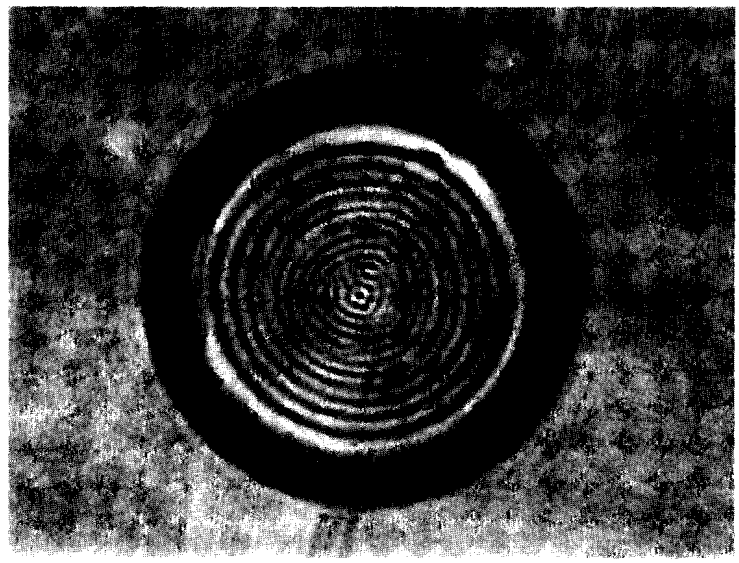

T913

Fig. 40.25(d)
Shadowgram of the same target produced by blocking the reference wave front. The rings appearing inside the image are believed to be due to Fresnel diffraction.

ACKNOWLEDGMENT

This work was supported by the the U.S. Department of Energy Office of Inertial Fusion under agreement No. DE-FC03-85DP40200 and by the Laser Fusion Feasibility Project at the Laboratory for Laser Energetics, which has the following sponsors: Empire State Electric Energy Research Corporation, New York State Energy Research and Development Authority, Ontario Hydro, and the University of Rochester. Partial support by the U.S. Department of Energy under agreement No. DE-AS08-99DP10782 is also acknowledged. Such support does not imply endorsement of the content by any of the above parties.

REFERENCES

1. D. L. Musinski *et al.*, *J. Vac. Sci. Technol. A* **5**, 2746 (1987).
2. LLE Review **31**, 114 (1987).
3. K. Kim, L. Mok, M. J. Erlenborn, and T. P. Bernat, *J. Vac. Sci. Technol. A* **3**, 1196 (1985).
4. K. Kim and D. L. Krahn, *J. Appl. Phys.* **61**, 2729 (1987).
5. T. P. Bernat, D. H. Darling, and J. J. Sanchez, *J. Vac. Sci. Technol.* **20**, 1362 (1982).
6. V. M. Izgorodin, S. B. Kormer, G. P. Nikolaev, and A. V. Pinegin, *Sov. J. Quantum Electron.* **16**, 35 (1986).
7. T. R. Pattinson and W. J. Felmlee, *J. Vac. Sci. Technol. A* **6**, 1882 (1988).
8. T. F. Powers and J. R. Miller, *J. Vac. Sci. Technol. A* **1**, 945 (1983).
9. J. A. Tarvin *et al.*, *Proc. SPIE* **192**, 239 (1979).
10. J. R. Miller and J. E. Sollid, *Appl. Opt.* **17**, 852 (1978).